JOURNAL OF COMPUTATIONAL PHYSICS **130,** 161–173 (1997)
ARTICLE NO. CP965561

Higher Order KFVS Algorithms Using Compact Upwind Difference Operators

K. S. Ravichandran

Flosolver Unit, CTFD Division, National Aerospace Laboratories, Bangalore, India
E-mail: ksravi@cmmacs.ernet.in

Received April 14, 1995; revised July 5, 1996

A family of high order accurate compact upwind difference operators have been used, together with the split fluxes of the KFVS (kinetic flux vector splitting) scheme to obtain high order semidiscretizations of the 2D Euler equations of inviscid gas dynamics in general coordinates. A TVD multistage Runge–Kutta time stepping scheme is used to compute steady states for selected transonic/supersonic flow problems which indicate the higher accuracy and low diffusion realizable in such schemes. © 1997 Academic Press

1. INTRODUCTION

It is generally a well accepted fact that accurate simulation of fluid flow with multiple and wide range of spatial scales and structures is a difficult task except through spectral approximations. However, the use of spectral approximations at present is limited by their applicability to simple geometries with generally periodic boundary conditions. While it is possible in principle to devise very high order accurate finite-difference approximations to the spatial derivatives occurring in the Euler or Navier–Stokes equations, recent studies [1] indicate that considerations based on mere formal accuracy (low truncation error) are not sufficient to ensure uniform resolution of the wide range of scales that may be present in the solution that one wants to approximate. In particular the smaller length scales are often poorly represented in the conventional high order difference approximations. While uniform resolution of the whole range of scales (ignoring aliasing errors) is exclusively the property of spectral methods, Lele has shown that it is possible to devise on a given stencil difference schemes that have much better resolution properties than conventional difference schemes of comparable order of accuracy. The price paid is that one is required in general to invert a tridiagonal system of linear equations to compute the derivatives. This class of difference approximations, which are called compact difference schemes, may be of the centered or upwind type and are classically known as rational function (as opposed to polynomial function) or Padé approximants to the derivatives. The high cost as well as the limited geometry adaptability of the spectral methods has in recent years given the impetus to investigate the effectiveness of compact difference approximations for a wide range of inviscid and viscous flow problems.

In the present paper we study a class of compact upwind difference approximations to the Euler equations of inviscid gas dynamics. The motivation is to investigate the suitability of these schemes for the computation of viscous transonic internal/external flows wherein isolated and/or interacting shock waves may be present giving rise to complex shock wave/boundary layer interaction zones. Since the viscous terms may be approximated to a high degree of accuracy by centered compact formulae, a prerequisite for accurate viscous computations is the sharp and monotone resolution of shock discontinuities in such flows. The present work is an attempt to study the suitability of compact schemes with this purpose in mind. The computational results reported here therefore are restricted to inviscid, high speed flows.

The compact upwind algorithms proposed in this paper preserve high order accuracy in the smooth regions, but reduce to first-order accuracy in the vicinity of shocks and other solution extrema because of the use of minmod flux limiters. Such a compromise is obviously unavoidable if one wants to prevent spurious, high frequency numerical oscillations from polluting the accuracy of the computed solution in such narrow transition regions. The centered compact approximations proposed in [1] are unsuitable for computing inviscid flows with discontinuities because of the odd–even decoupling which gives rise to high frequency oscillations even in smooth regions. Killing such oscillations requires the introduction of commensurately high order background dissipation terms, which implies that the compactness of the stencil is lost. On the other hand, as found by Cockburn and Shu [10], introduction of minmod limiters in centered schemes, affects the solution accuracy even in smooth regions if there are oscillations there to suppress. The use of compact upwind operators together with the KFVS split fluxes [2] is motivated by these consid-

0021-9991/97 $25.00

erations. Another reason behind the choice of KFVS splitting is that, as compared to the van Leer or Steger–Warming splittings which have vanishing eigenvalues, the former is expected to maintain its robustness in high order computations of mixed flow fields with sonic points present.

From a different point of view, the present work may be viewed as an approach to generating high order KFVS schemes on structured meshes. Since the schemes are formulated in a finite-volume framework with the equations cast in strong conservation form, Lax–Wendroff theorem guarantees that limit solutions are indeed weak solutions to the conservation laws, the Euler equations in the present case. Additionally, use of the entropy consistent KFVS splitting [2] results in a family which has been used to compute transonic flow solutions that are free of sonic glitches or expansion shocks. Hence there is reason to believe, and numerical experience confirms, that the present higher order extensions of the KFVS formalism using compact upwind operators does remain entropy consistent.

It is pertinent to mention here that upwinding in compact schemes has earlier been incorporated by Tolstykh [3, 4] through a Murman type switch. This gives rise to compact schemes that are Riemann solver based and, hence, of the flux-difference splitting type. A generalization of this approach to other approximate Riemann solvers was proposed in [5] and its extension to a finite-volume framework in general coordinates may be found in [6]. Transonic flow computations using Roe's approximate Riemann solver [7] showed that while crisp shock capture is possible, computation times are uneconomical basically because the algorithm involves the inversion of block tridiagonal linear systems whose subblocks (4×4 in the case of 2D Euler equations) are dense. As opposed to this drawback of the FDS-based compact schemes, the present approach based on flux-vector splitting gives rise to subblocks which are diagonal matrices with constant entries. In some cases the tridiagonal linear system only involves a Toeplitz matrix and therefore may be inverted by special faster algorithms. In any case the effort involved in the inversion and the computation of the high order accurate derivatives is now only proportional to m and not to its power (m being the number of dependent variables).

Steady state compressible flow calculations using fourth-order centered compact schemes with or without artificial dissipation have been carried out by Abarbanel and Kumar [8]. Oblique shock reflection computations show that the computed solution is oscillatory, basically because flux limiters were not introduced near discontinuities. Applying a fourth-order compact operator to the conventional MacCormack scheme, Carpenter [9] has concluded that the resulting upwind C-Mac scheme gives considerable improvement in accuracy for the supersonic mixing layer problem. More recently Cockburn and Shu [10] have formulated a family of nonlinearly stable compact schemes for nonlinear scalar conservation laws in one and two space dimensions, introducing upwinding through flux-vector splitting. In spite of the BV-stability property, they found that their centered approximations fared badly in terms of accuracy in actual computations because of the odd–even decoupling problem mentioned above. This motivates the emphasis on the use of upwind compact operators in the present work. Thus the present approach is essentially similar to theirs though modifications have been necessitated from the point of view of computational economy. Also while the restriction in [10] to the class of symmetric compact operators and the introduction of a solution mean enables them to prove results concerning formal accuracy in the scalar case, we use a wider class of compact upwind operators which do not possess such symmetry. Formal accuracy of the flux-limited scheme therefore remains unverified for the present. However, nonlinear TVD stability of the flux-limited semidiscrete scheme is easily established following Tadmor [15].

Halt and Agarwal [16] have also computed Euler solutions for the Ringleb problem and a ramp problem using a compact high order characteristic based method. Their scheme requires the introduction of higher derivatives and moments of the governing equations. A compact reconstruction polynomial is used to obtain the left and right states at cell interfaces in the MUSCL spirit and the numerical flux is computed from a pseudo 1D Riemann solver. No computations have been reported for flows with discontinuities. Compressible viscous flow computations for the supersonic mixing layer using third- and fifth-order compact schemes have also been reported by Ma and Fu [11]. They have used the Steger–Warming flux-splitting for upwinding. Although no comparisons have been made, computed results show the capture of sharp shock transitions and smooth rollup structures.

In what follows, the numerical scheme for the Euler equations in one space dimension is described and then extended in a finite-volume framework to two dimensions in general curvilinear coordinates. The algorithm is applied to compute solutions to inviscid transonic/supersonic flows. Validation is shown by computational comparisons with results obtained from well known second-order upwind TVD schemes [12].

2. HIGH ORDER COMPACT UPWIND SPATIAL DISCRETIZATION

The Euler equations in one-space dimension may be written as

$$\frac{\partial U}{\partial t} + \frac{\partial F}{\partial x} = 0, \tag{2.1}$$

where $U = [\rho, \rho u, e]^t$ and $F = [\rho u, \rho u^2 + p, (e + p)u]^t$. The symbols ρ, u, e, and p denote respectively the density, gas speed, total energy, and pressure.

The flux F may be split as a sum of positive and negative components; i.e., $F = F^+ + F^-$ such that the Jacobians $\partial F^+/\partial U$ and $\partial F^-/\partial U$ respectively have nonnegative and nonpositive eigenvalues throughout the flow domain. Equation (2.1) may then be rewritten as

$$\frac{\partial U}{\partial t} + \frac{\partial F^+}{\partial x} + \frac{\partial F^-}{\partial x} = 0. \tag{2.2}$$

Let the domain be $(0 \le x \le 1)$ and set up the grid $x_j = j\,\Delta x$, $j = 0, 1, 2, \ldots, N$, $\Delta x = 1/N$. A first-order accurate semidiscretization may be now obtained by using two point backward differences for the positive part of the flux and forward differences for the negative part,

$$\frac{1}{h}\Delta_- F_j^+ = \partial_x F_j^+ + O(h) \tag{2.3a}$$

$$\frac{1}{h}\Delta_+ F_j^- = \partial_x F_j^- + O(h), \tag{2.3b}$$

where $\Delta_\pm$ are the two point forward and backward difference operators, respectively. A conservative semidiscretization of (2.2) is written in the form

$$\frac{\partial U_j}{\partial t} + (\hat{F}_{j+1/2} - \hat{F}_{j-1/2})/h = 0, \tag{2.4a}$$

where h is the mesh spacing and the numerical flux $\hat{F}_{j+1/2}$ corresponding to the first-order upwind formulae (2.3a), (2.3b) is given by

$$\hat{F}_{j+1/2} = F^+(U_j) + F^-(U_{j+1}). \tag{2.4b}$$

Third-order accuracy in smooth regions may be realized using the compact difference relations

$$\frac{1}{h}\Delta_- F_j^+ = A_+ \partial_x F_j^+ + O(h^3) \tag{2.5a}$$

$$\frac{1}{h}\Delta_+ F_j^- = A_- \partial_x F_j^- + O(h^3), \tag{2.5b}$$

where $A_+ = (5, 8, -1)/12$ and $A_- = (-1, 8, 5)/12$. A three-point grid function operator may be interpreted as $(a, b, c)f_j = af_{j-1} + bf_j + cf_{j+1}$. Denoting the elements of the operator A_+ by (a_1, a_2, a_3), note that $A_- = (a_3, a_2, a_1)$. This is a property shared by all schemes considered in this paper. Once a numerical flux similar to (2.4b) or, more conveniently, difference quotients as in (2.3a), (2.3b) are given, it is easy to find the corresponding compact operators $A_\pm$ possessing the property mentioned above. For certain choices of the numerical flux, such as that of Cockburn and Shu below, it turns out that $a_1 = a_3$ so that $A_+ = A_-$. This fact is used for establishing higher order accuracy of the flux-limited schemes in smooth regions away from the extrema; see [10]. Using (2.5a), (2.5b) in (2.2), we obtain a third-order accurate semidiscretization,

$$\left(\frac{\partial U}{\partial t}\right)_j + A_+^{-1}\left(\frac{1}{h}\Delta_- F_j^+\right) + A_-^{-1}\left(\frac{1}{h}\Delta_+ F_j^-\right) = 0. \tag{2.6}$$

It is now convenient to recast (2.6) in the conservation form (2.4) with the third-order numerical flux defined as

$$\hat{F}_{j+1/2} = A_+^{-1}(F^+(U_j)) + A_-^{-1}(F^-(U_{j+1})). \tag{2.7}$$

Equation (2.7) suggests that a general higher order numerical flux corresponding to any compact difference operator may be decomposed into positive and negative parts given by

$$\hat{F}_{j+1/2}^+ = A_+^{-1}(F_{j+1/2}^+);\ \hat{F}_{j+1/2}^- = A_-^{-1}(F_{j+1/2}^-) \tag{2.8a}$$

$$F_{j+1/2}^+ = b_1 F_{j-1}^+ + b_2 F_j^+ + b_3 F_{j+1}^+ + b_4 F_{j+2}^+ \tag{2.8b}$$

$$F_{j+1/2}^- = b_4 F_{j-1}^- + b_3 F_j^- + b_2 F_{j+1}^- + b_1 F_{j+2}^-. \tag{2.8c}$$

The coefficients b_k in (2.8b), (2.8c) satisfy the consistency condition $\sum b_k = 1$. A similar condition holds for the elements of the operators $A_\pm$. Depending on the choice of these coefficients, one may either obtain purely upwind (as in (2.7)) or centered but upwind weighted numerical fluxes. Of course (2.8a) (2.8b) also include fully centered fluxes but the choice of these schemes, even with flux limiters as in [10] in the computation of inviscid flows with discontinuities is not advisable because odd–even decoupling gives rise to high frequency oscillations even in smooth regions. The application of minmod limiters in such regions results in a global reduction in the order of accuracy. The presence of diffusive terms in viscous calculations may, however, mitigate this problem typical of centered schemes and may improve the solution quality and accuracy. As for the operator A corresponding to a choice of b's, attention here is restricted to those b's for which A remains tridiagonal. Some of the possible schemes are listed below:

(1) Third-order compact scheme with one point upwind numerical flux (Tolstykh): $b_1 = b_3 = b_4 = 0$, $b_2 = 1$; $a_1 = \frac{5}{12}$, $a_2 = \frac{8}{12}$, $a_3 = -\frac{1}{12}$.

(2) Third-order compact scheme with 2-point fully upwind flux (Cockburn and Shu): $b_1 = -\frac{1}{2}$, $b_2 = \frac{3}{2}$, $b_3 = b_4 = 0$; $a_1 = -\frac{1}{3}$, $a_2 = \frac{5}{3}$, $a_3 = -\frac{1}{3}$.

(3) Third-order compact scheme with 2-point upwind weighted flux (Ma and Fu): $b_1 = 0$, $b_2 = \frac{5}{6}$, $b_3 = \frac{1}{6}$, $b_4 = 0$; $a_1 = \frac{1}{3}$, $a_2 = \frac{2}{3}$, $a_3 = 0$.

(4) Fifth-order compact scheme with 4-point upwind weighted flux (Ma and Fu): $b_1 = \frac{3}{60}$, $b_2 = \frac{47}{60}$, $b_3 = \frac{11}{60}$, $b_4 = -\frac{1}{60}$; $a_1 = \frac{2}{5}$, $a_2 = \frac{3}{5}$, $a_3 = 0$.

Scheme 1 is similar to that of Tolstykh [13] while scheme 2 is the only upwind scheme listed by Cockburn and Shu [10]. Schemes 3 and 4 have been used by Ma and Fu [11] for supersonic mixing layer calculations. As mentioned earlier the A operator is symmetric for scheme 2. Further, the matrix operator A is strictly diagonally dominant for all schemes mentioned above (and satisfies Lemma 2.2 of [10]), so that the inversion indicated in (2.7) can be carried out.

The residual may be defined by

$$R_j = (\hat{F}_{j+1/2} - \hat{F}_{j-1/2})/h = \partial_x F_j^+ + \partial_x F_j^-, \tag{2.9}$$

where the interface flux is given by

$$\hat{F}_{j+1/2} = \hat{F}^+_{j+1/2} + \hat{F}^-_{j+1/2}. \tag{2.10}$$

The tridiagonal linear system indicated in (2.8a) involves only constant matrices that are independent of the grid point or the time step. Also for the case of a system of equations, the submatrices in the block tridiagonal system are diagonal and, hence, are easily inverted. This is in contrast to the block tridiagonal linear system arising in [7], where the submatrices are solution dependent and dense and hence are very expensive to invert. The semidiscrete system (2.4a) and (2.9) may be integrated using a multistage TVD Runge–Kutta scheme [10].

The number of boundary conditions specified at $j = 0$ and $j = N$ correspond to the number of incoming characteristics which may be less than or equal to 3 for the case of 1D Euler equations. Assume that appropriate boundary conditions are specified at $j = 0$ and N. In that case for a general initial boundary value problem (IBVP) dummy points may be introduced at $j = -1, -2$ and $j = N + 1$, $N + 2$, and values assigned for the components of U at these points in such a manner that the specified boundary conditions at $j = 0$ and N are fulfilled. The numerical flux given by (2.10) may therefore be evaluated for j in $0 \le j \le N$. Hence,

$$A_+ \hat{F}^+_{j+1/2} = F^+_{j+1/2} \tag{2.11a}$$

$$F^+_{j+1/2} = b_1 F^+_{j-1} + b_2 F^+_j + b_3 F^+_{j+1} + b_4 F^+_{j+2}. \tag{2.11b}$$

It is apparent from (2.11a) that if suitable values are specified at the dummy cells $j = -1, -2, N + 1$, and $N + 2$ the linear tridiagonal system (2.11a) may be closed by setting $\hat{F}^+_{-1/2} = F^+_{-1/2}$. Similarly at the boundary N, $\hat{F}^+_{N+1/2} = F^+_{N+1/2}$, assuming that the boundary values at $N + 1$ and $N + 2$ have been specified. A similar procedure works for the evaluation of the higher order negative flux. Representing the operators A_+ by (a_j, b_j, c_j) (2.11a) may be written in expanded form as

$$\begin{aligned}\mathrm{diag}(a_j)\hat{F}^+_{j-1/2} + \mathrm{diag}(b_j)\hat{F}^+_{j+1/2} \\ + \mathrm{diag}(c_j)\hat{F}^+_{j+3/2} = F^+_{j+1/2},\end{aligned} \tag{2.11c}$$

where the RHS is evaluated from (2.11b). Having obtained $\hat{F}^+_{j+1/2}$ and $\hat{F}^-_{j+1/2}$, the residual is computed from (2.9 to 2.10). However, the resulting scheme is not nonoscillatory and it is necessary to limit the higher order fluxes at solution extrema. Equations (2.9), (2.10) are, hence, replaced by

$$d\hat{F}^+_{j+1/2} = \hat{F}^+_{j+1/2} - F^+_j; \quad d\hat{F}^-_{j+1/2} = F^-_{j+1} - \hat{F}^-_{j+1/2} \tag{2.12a}$$

$${}^{(m)}d\hat{F}^+_{j+1/2} = \mathrm{minmod}(d\hat{F}^+_{j+1/2}, \Delta_+ F^+_j, \Delta_+ F^+_{j-1}) \tag{2.12b}$$

$${}^{(m)}d\hat{F}^-_{j+1/2} = \mathrm{minmod}(d\hat{F}^-_{j+1/2}, \Delta_+ F^-_j, \Delta_+ F^-_{j+1}) \tag{2.12c}$$

$${}^{(m)}\hat{F}^+_{j+1/2} = F^+_j + {}^{(m)}d\hat{F}^+_{j+1/2} \tag{2.12d}$$

$${}^{(m)}\hat{F}^-_{j+1/2} = F^-_{j+1} - {}^{(m)}d\hat{F}^-_{j+1/2} \tag{2.12e}$$

$${}^{(m)}\hat{F}_{j+1/2} = {}^{(m)}\hat{F}^+_{j+1/2} + {}^{(m)}\hat{F}^-_{j+1/2} \tag{2.12f}$$

$$R_j = ({}^{(m)}\hat{F}_{j+1/2} - {}^{(m)}\hat{F}_{j-1/2})/h, \tag{2.12g}$$

where the minmod limiter function vanishes if any of the arguments differ in sign and otherwise assumes the value of the argument with least absolute value. The resulting scheme is of course first-order accurate at solution extrema.

The spatial discretization as described above is similar to that described for scalar equations by Cockburn and Shu in [10]. They, however, carryout a premultiplication by the compact difference operator A thereby defining a mean value for U. As a result their first-order flux differences (appearing in (2.12b), (2.12c)) are defined in terms of this mean value and this results in multiple evaluation of the Euler fluxes as is evident for (2.12a). Whle their formulation enables them to establish TVB stability results for scalar conservation laws, the present scheme is more economical in practical computations. Second, the operator A is not required to be symmetric, which gives a wider choice of the parameters b_k to evaluate the cell face fluxes given by (2.8b), (2.8c).

Despite the departures from the algorithms of Cockburn and Shu, as mentioned above, without any additional restrictions on the compact operator A, the present scheme with the limiters (2.12) may be shown to be TVD in the 1D case for the scalar conservation law. To this end we follow Tadmor [15, p.1004, Eq. (2.10)], who shows that for

a semidiscrete scheme written in the incremental form, nonnegativity of the incremental coefficients is sufficient to ensure the TVD property.

PROPOSITION. *For the case of a scalar conservation law given by* (2.1), *the semi-discrete scheme* (2.4a) *with numerical flux given by* (2.12a)–(2.12g) *is TVD.*

Proof. The net numerical flux can be written in the incremental form as

$$\begin{aligned}\hat{F}_{j+1/2} - \hat{F}_{j-1/2} &= {}^{(m)}\hat{F}_{j+1/2} - {}^{(m)}\hat{F}_{j-1/2} \\ &= F_j^+ + {}^{(m)}d\hat{F}_{j+1/2}^+ + F_{j+1}^- - {}^{(m)}d\hat{F}_{j+1/2}^- \\ &\quad - F_{j-1}^+ - {}^{(m)}d\hat{F}_{j-1/2}^+ - F_j^- + {}^{(m)}d\hat{F}_{j-1/2}^- \\ &= \Delta_+ F_{j-1}^+ + {}^{(m)}d\hat{F}_{j+1/2}^+ - {}^{(m)}d\hat{F}_{j-1/2}^+ \\ &\quad + \Delta_+ F_j^- - {}^{(m)}d\hat{F}_{j+1/2}^- + {}^{(m)}d\hat{F}_{j-1/2}^- \\ &= -C_{j+1/2}\Delta_+ u_j + D_{j-1/2}\Delta_+ u_{j-1},\end{aligned}$$

where

$$\begin{aligned}C_{j+1/2} &= -(\Delta_+ F_j^- - {}^{(m)}d\hat{F}_{j+1/2}^- + {}^{(m)}d\hat{F}_{j-1/2}^-)/\Delta_+ u_j \\ D_{j-1/2} &= (\Delta_+ F_{j-1}^+ + {}^{(m)}d\hat{F}_{j+1/2}^+ - {}^{(m)}d\hat{F}_{j-1/2}^+)/\Delta_+ u_{j-1}.\end{aligned}$$

The limiters (2.12a)–(2.12g), together with the Lax–Friedrich flux splitting, clearly imply that the coefficients

$$C_{j+1/2} \geq 0, \quad D_{j+1/2} \geq 0 \quad \text{for all } j.$$

To see this for $D_{j+1/2}$, using the minmod limiters, one obtains

$$\begin{aligned}{}^{(m)}d\hat{F}_{j+1/2}^+ &= \text{minmod}(d\hat{F}_{j+1/2}^+, \Delta_+ F_j^+, \Delta_+ F_{j-1}^+) \\ {}^{(m)}d\hat{F}_{j-1/2}^+ &= \text{minmod}(d\hat{F}_{j-1/2}^+, \Delta_+ F_{j-1}^+, \Delta_+ F_{j-2}^+),\end{aligned}$$

by virtue of the Lax–Friedrich splitting $\Delta_+ F_{j-1}^+/\Delta_+ u_{j-1} \geq 0$.

If $\Delta_+ u_{j-1} > 0$, then $\Delta_+ F_{j-1}^+ \geq 0 \Rightarrow {}^{(m)}d\hat{F}_{j+1/2}^+ \geq 0$ and ${}^{(m)}d\hat{F}_{j-1/2}^+ \geq 0$ by definition of the minmod operator. Now

$$\begin{aligned}&{}^{(m)}d\hat{F}_{j-1/2}^+ = 0 \Rightarrow D_{j-1/2} = (\Delta_+ F_{j-1}^+ + {}^{(m)}d\hat{F}_{j+1/2}^+)/\Delta_+ u_{j-1} \geq 0, \\ &{}^{(m)}d\hat{F}_{j-1/2}^+ > 0 \Rightarrow {}^{(m)}d\hat{F}_{j-1/2}^+ < (\Delta_+ F_{j-1}^+ \leq \Delta_+ F_{j-1}^+ + {}^{(m)}d\hat{F}_{j+1/2}^+ \\ &\Rightarrow D_{j-1/2} = (\Delta_+ F_{j-1}^+ + {}^{(m)}d\hat{F}_{j+1/2}^+ - {}^{(m)}d\hat{F}_{j-1/2}^+)/\Delta_+ u_{j-1} \geq 0.\end{aligned}$$

If $\Delta_+ u_{j-1} < 0$, then $\Delta_+ F_{j-1}^+ < 0 \Rightarrow {}^{(m)}d\hat{F}_{j+1/2}^+ \leq 0$ and ${}^{(m)}d\hat{F}_{j-1/2}^+ \leq 0$. Then

$$\begin{aligned}&{}^{(m)}d\hat{F}_{j-1/2}^+ = 0 \Rightarrow D_{j-1/2} = (\Delta_+ F_{j-1}^+ + {}^{(m)}d\hat{F}_{j+1/2}^+)/\Delta_+ u_{j-1} \geq 0 \\ &{}^{(m)}d\hat{F}_{j-1/2}^+ < 0 \Rightarrow {}^{(m)}d\hat{F}_{j-1/2}^+ \geq (\Delta_+ F_{j-1} \geq \Delta_+ F_{j-1}^+ + {}^{(m)}d\hat{F}_{j+1/2}^+ \\ &\Rightarrow D_{j-1/2} = (\Delta_+ F_{j-1}^+ + {}^{(m)}d\hat{F}_{j+1/2}^+ - {}^{(m)}d\hat{F}_{j-1/2}^+)/\Delta_+ u_{j-1} \geq 0.\end{aligned}$$

Thus D is nonnegative. In a similar manner it may be shown that $C_{j+1/2} \geq 0$ and the proof is complete.

It should be noted that the above result is stronger than Proposition 2.3 of [10] which establishes TVB property with an additional condition on the compact difference operators A.

The KFVS split fluxes are given by [14]

$$\begin{aligned}F^\pm &= [\rho u a^\pm \pm \rho b, (p + \rho u^2)a^\pm \pm \rho u b, (e + p)u a^\pm \\ &\quad \pm (p/2 + e)b]^t = [f^\pm, u f^\pm + p a^\pm, H f^\pm \mp p b/2]^t \quad (2.13) \\ &\quad \text{with } f^\pm = \rho u a^\pm \pm \rho b.\end{aligned}$$

The quantities $a^\pm = (1 \pm \text{erf}(s(u))/2$, $b = \exp(-(s(u))^2)/2(\pi\beta)^{1/2}$, $s(x) = x\beta^{1/2}$, and $\beta = \rho/2p$, where $\text{erf}(\cdot)$ denotes the error function. The total enthalpy $H = (e + p)/\rho$. It is obvious that in place of (2.13) one may use any other flux splitting. However the tridiagonal inversion required to compute the higher order fluxes implies that upwinding can be ensured only with those splittings such that the associated flux Jacobians (i) have eigenvalues of the same sign and (ii) the sign of the eigenvalues is independent of the flow.

3. EXTENSION TO TWO DIMENSIONS IN GENERAL COORDINATES

The Euler equations in two dimensions in general coordinates may be written as

$$\frac{\partial \hat{U}}{\partial t} + \frac{\partial \tilde{F}}{\partial \xi} + \frac{\partial \tilde{G}}{\partial \eta} = 0, \tag{3.1}$$

where $\hat{U} = U/J$, $\tilde{F} = (\xi_x F + \xi_y G)/J$, $\tilde{G} = (\eta_x F + \eta_y G)/J$, and $J = (\xi_x \eta_y - \xi_y \eta_x)$ is the Jacobian of the transformation. We assume that $J \neq 0$. The state vector $U = [\rho, \rho u, \rho v, e]^t$, and the fluxes $F = [\rho u, \rho u^2 + p, \rho uv, (e + p)u)]^t$, and $G = [\rho v, \rho uv, \rho v^2 + p, (e + p)v]^t$, where ρ, u, v, p, and e are the density, x-component of velocity, y-component of velocity, the pressure, and the total energy, respectively. e and p are connected through $e = p/(\gamma - 1) + \rho(u^2 + v^2)/2$. As in the 1D case the fluxes $\tilde{F}$ and $\tilde{G}$ are split and written as a sum of positive and negative parts. Denoting these by $\tilde{F}^\pm$ and $\tilde{G}^\pm$, respectively, and rewriting (3.1) as

$$\frac{\partial \hat{U}}{\partial t} + \frac{\partial \tilde{F}^+}{\partial \xi} + \frac{\partial \tilde{F}^-}{\partial \xi} + \frac{\partial \tilde{G}^+}{\partial \eta} + \frac{\partial \tilde{G}^-}{\partial \eta} = 0, \tag{3.2}$$

it is natural to use upwind weighted differencing for the positive and negative flux derivatives. Higher order accuracy is subsequently achieved by using the compact difference relations for the ξ and η directions. Typically,

$$A^{\xi}_{\pm}\hat{F}^{\pm}_{i+1/2} = \tilde{F}^{\pm}_{i+1/2} \tag{3.3a}$$

$$\tilde{F}^{+}_{i+1/2} = b_1\tilde{F}^{+}_{i-1} + b_2\tilde{F}^{+}_{i} + b_3\tilde{F}^{+}_{i+1} + b_4\tilde{F}^{+}_{i+2} \tag{3.3b}$$

$$\tilde{F}^{-}_{i+1/2} = b_4\tilde{F}^{-}_{i-1} + b_3\tilde{F}^{-}_{i} + b_2\tilde{F}^{-}_{i+1} + b_1\tilde{F}^{-}_{i+2} \tag{3.3c}$$

which can be written in expanded form as

$$a^{\xi}_i\hat{F}_{i-1/2} + b^{\xi}_i\hat{F}_{i+1/2} + c^{\xi}_i\hat{F}_{i+3/2} = \tilde{F}_{i+1/2}, \quad 0 \le i \le i_{\max}. \tag{3.4}$$

In Eq. (3.4) the $\pm$ or $\mp$ signs and the j subscript have been dropped for convenience. Note that the block tridiagonal system (3.4) has to be solved for every j, $0 \le j \le j_{\max}$. (It is assumed that the computational domain $(0, 1) \times (0, 1)$ in mapped coordinates has been partitioned into a mesh with $\Delta\xi = 1/i_{\max}$ and $\Delta\eta = 1/j_{\max}$). Fortunately as in the 1D case, the block matrices which are 4×4, are diagonal with constant diagonal entries and therefore the inversion of (3.4) entails no more effort than a simple, scalar tridiagonal system. An equation similar to (3.4) may be written for the η-direction and these will have to be solved for every i, $0 \le i \le i_{\max}$. Having solved for $\hat{F}^{\pm}_{i+1/2,j}$ and $\hat{G}^{\pm}_{i,j+1/2}$, the total residual is defined by

$$\hat{F}_{i+1/2,j} = \hat{F}^{+}_{i+1/2,j} + \hat{F}^{-}_{i+1/2,j} \tag{3.5a}$$

$$\hat{G}_{i,j+1/2} = \hat{G}^{+}_{i,j+1/2} + \hat{G}^{-}_{i,j+1/2} \tag{3.5b}$$

$$R_{ij} = (\hat{F}_{i+1/2,j} - \hat{F}_{i-1/2,j})/\Delta\xi + (\hat{G}_{i,j+1/2} - \hat{G}_{i,j-1/2})/\Delta\eta. \tag{3.5c}$$

As in the 1D formulation, the high order cell interface fluxes may be limited and replaced by a sequence of formulae given by (2.12a)–(2.12g) for each of the coordinate directions ξ and η. The limited fluxes may then be used in (3.5c) to evaluate the residual.

The semidiscrete approximation for (3.1) may now be written as

$$\partial\hat{U}/\partial t + R_{ij} = 0 \tag{3.6}$$

which may now be integrated by a multistage TVD Runge–Kutta scheme. As in the one-dimensional case it is assumed that proper boundary values are specified at the dummy points $i = -2, -1$ and $i = i_{\max} + 1, i_{\max} + 2$ for $\forall j$ and $j = -2, -1$ and $j = j_{\max} + 1, j_{\max} + 2$ for $\forall i$ so that the block tridiagonal systems (3.4) may be closed by suitable first-order approximations for the net numerical flux at the boundaries thus making the solution of (3.4) possible. Such a boundary approximation implies that the higher order accuracy of the interior scheme is not maintained at the boundary. Numerical experiments show that, while this does not unduly affect the accuracy of the local solution whenever the latter is close to uniform conditions (such as farfield boundaries), near solid wall boundaries the accuracy of the computed solution appears to be satisfactory. The present first-order approximation at the boundary at least has the merit that the boundary scheme is reasonably robust and stable. Stable higher order boundary approximations ought to be investigated in the future. It now remains to specify the KFVS split fluxes in the curvilinear coordinates.

Define the unit normals and the contravariant velocities as

$$k = (\xi_x^2 + \xi_y^2)^{1/2}, \quad (\hat{\xi}_x, \hat{\xi}_y) = (\xi_x, \xi_y)/k, \quad \hat{u} = \hat{\xi}_x u + \hat{\xi}_y v$$
$$l = (\eta_x^2 + \eta_y^2)^{1/2}, \quad (\hat{\eta}_x, \hat{\eta}_y) = (\eta_x, \eta_y)/l, \quad \hat{v} = \hat{\eta}_x u + \hat{\eta}_y v;$$

KFVS splitting as

$$\begin{aligned}
&\tilde{F}^{\pm} = [\tilde{f}^{\pm}, \tilde{f}^{\pm}u + \hat{\xi}_x pa^{\pm}, \tilde{f}^{\pm}v + \hat{\xi}_y pa\pm, \tilde{f}^{\pm}H \mp pb/2]^t \\
&\tilde{G}^{\pm} = [\tilde{g}^{\pm}, \tilde{g}^{\pm}u + \hat{\eta}_x pc^{\pm}, \tilde{g}^{\pm}v + \hat{\eta}_y pc^{\pm}, \tilde{g}^{\pm}H \mp pd/2]^t \\
&\tilde{f}^{\pm} = \rho\hat{u}a^{\pm} \pm \rho b, \tilde{g}^{\pm} = \rho\hat{v}c^{\pm} \pm \rho d \\
&a^{\pm} = (1 \pm \mathrm{erf}(s(\hat{u})))/2, \qquad c^{\pm} = (1 \pm \mathrm{erf}(s(\hat{v})))/2 \\
&b = \exp(-(s(\hat{u}))^2)/2(\pi\beta)^{1/2}, \quad d = \exp(-(s(\hat{v}))^2)/2(\pi\beta)^{1/2}.
\end{aligned} \tag{3.7}$$

The definitions of $s(x)$, β, etc. remain the same as in the 1D case.

Boundary Conditions

For the problems considered in this work, three types of boundary conditions, namely, farfield, inflow/outflow, and solid wall, are encountered. On a solid wall for inviscid flow, it is necessary to satisfy the zero normal velocity boundary condition. Since the present scheme is of the cell-centered type, the solid wall forms a cell interface between the cell (say) $j = 1$ and $j = 0$, the latter being the first of the two dummy cells. A simple way to satisfy the zero normal velocity condition on the cell interface is to use the reflection principle (ρ, $\rho\hat{v}$, and e are symmetric and $\rho\hat{u}$ is antisymmetric across the cell interface, $\hat{u}$ and $\hat{v}$ being the local normal and tangential components of the velocity vector). This way the values of the state vector in any number of dummy cells may be specified. Since the computation of cell-interface numerical fluxes is similar to using an approximate 1D Riemann solver, this procedure remains valid as long as the deviation of the local grid lines from orthogonality is small.

At the farfield, values for the dummy cells are found by treating the flow locally as 1D and using the theory of 1D Riemann invariants. At a subsonic inflow boundary, for example, free stream values are assigned for the three incoming Riemann invariants and the fourth, computed by extrapolation from the interior. At a subsonic outflow

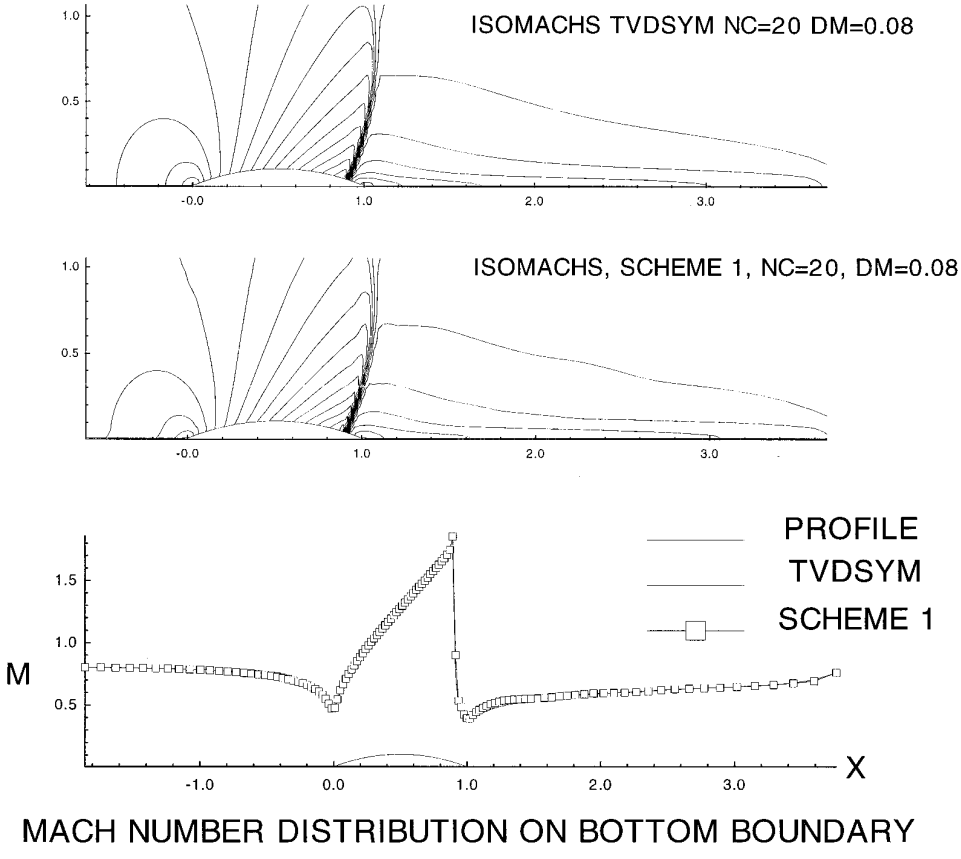

FIG. 1. $M = 0.85$. External flow past prabolic profile.

boundary, only one boundary condition is required, which may be chosen to be, pressure. The other three unknowns are extrapolated from the interior. At a supersonic inflow boundary all cells are assigned freestream values while at the outflow, all values are extrapolated to zeroth order from the interior. Also a boundary point is called subsonic or supersonic according as q/c is greater or less than unity, where q is the gas speed and c the speed of sound. The normal component of q evaluated locally is then used to determine whether the boundary is inflow or outflow.

In channel flow calculations the left boundary is always treated as inflow and the right boundary as outflow. This implies that reverse flow at these boundaries is not permissible. Inflow and outflow boundary conditions are treated exactly in the same manner as explained above for the farfield, except that inflow conditions are substituted for freestream values and exit pressure is specified when required.

The solution in every case is started impulsively. This leads to large transients in the early stages of the time-marching procedure and the calculations may break down for high Mach numbers due to the occurrence of negative pressure or density even within the stable CFL number range. For the transonic to moderate supersonic Mach numbers considered in the present calculations, an impulsive start seems to pose no serious problems.

5. NUMERICAL RESULTS

The algorithm described above has been coded in FORTRAN and run on the ALPHA 3000 machine at the VAX computing facility at NAL. Computations have been done for external flow past (i) a 10% semithickness parabolic profile at transonic Mach numbers of 0.85 and 1.3, (ii) internal flow past a 4% parabolic hump at a Mach number of 1.4, (iii) $M = 3$ flow in converging diverging type channel, and (iv) Mach 3 supersonic flow past a curved concave wall. The choice of these case studies for algorithm validation will be justified below. A feature of the present computations is that comparisons have been made with conventional second-order symmetric or upwind TVD scheme (Harten–Yee) using the same computer code. Therefore flow initialization, grid and associated metric quantities, and boundary condition implementation are identical for all the computations reported here.

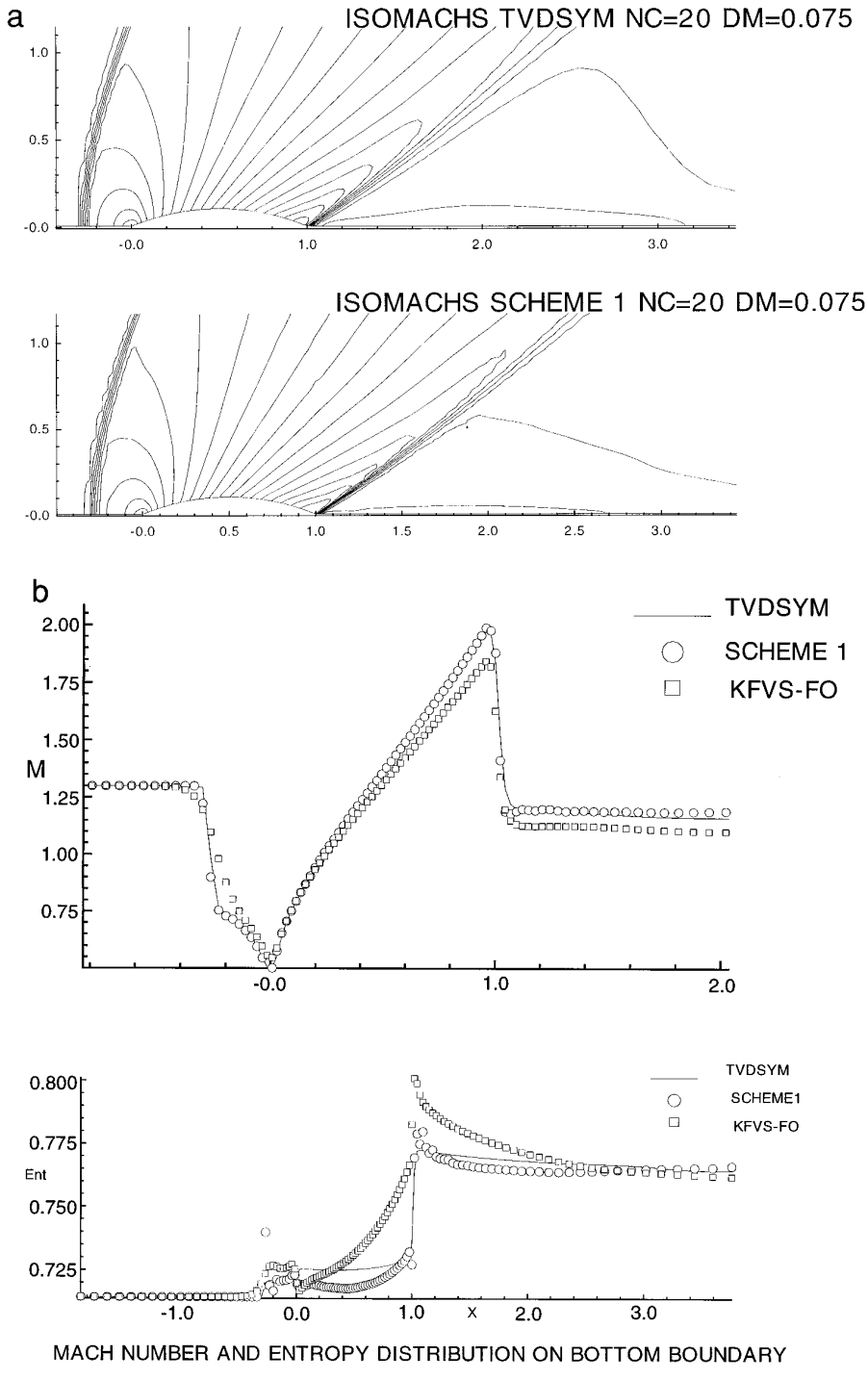

FIG. 2. $M = 1.3$. External flow past parabolic profile.

PROBLEM 1. Figure 1 shows results of computations for a subsonic freestream Mach number of 0.85. The profile has 10% semithickness. The 120×60 computational grid extends about three chords upstream and downstream of the profile and about four chords in the transverse direction. The results are presented in the form of Mach contours and surface distributions of the Mach number. Figure 1 shows a comparison of the results of second-order accurate TVDSYM computations [12] with that of CUD-TOL (scheme 1) which is third-order accurate. The Mach con-

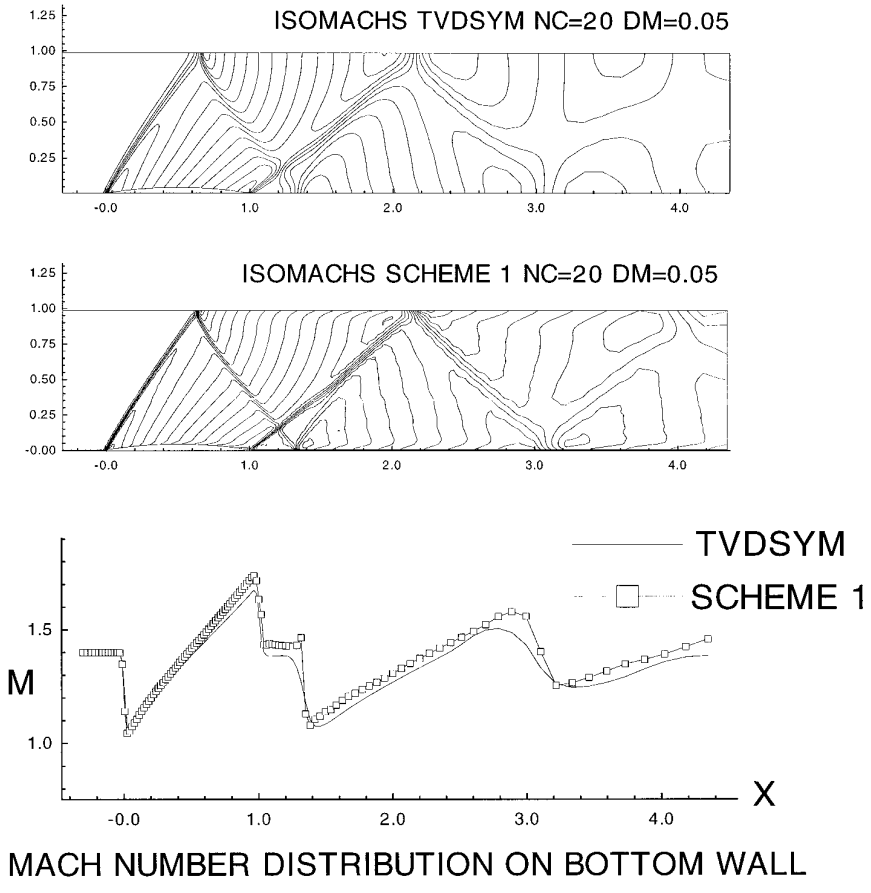

FIG. 3. $M = 1.4$. Flow past 4% parabolic bump in channel.

tours show that the shock is almost normal and well aligned locally with the grid. The shock transition on the surface is fairly sharp and free of over- or under-shoots.

PROBLEM 2. This concerns Mach 1.3 free air flow past the same profile. The grid in this case extends about one chord upstream and three chords downstream. The transverse extent of the grid is the same as in the previous case. For the specified Mach number and geometry, a detached shock forms upstream of the profile. An oblique shock forms at the trailing edge so that in this problem we can see the effects of shock misalignment with the grid. Figure 2a shows the Mach contours from the second-order TVDSYM scheme [12] compared with CUD-TOL, scheme 1 calculations. The detached shock ahead of the leading edge and the oblique shock at the trailing edge are captured well. Note that the respective computed maxima and minima of the Mach number field are in close agreement. Figure 2b shows the comparisons for surface Mach number and entropy distributions. While the Mach number distribution shows that the CUD-TOL shock transitions are slightly sharper; as expected, the surface entropy distribution is nonmonotone in the vicinity of the shocks. Such behavior in the entropy distribution has also been observed in third-order ENO [17] as well as to a minor extent in second-order TVD computations [18]. In Fig. 2b, the Mach number distribution obtained from a first-order KFVS computation is also included. It is apparent that higher dissipation in the vicinity of the shock affects the accuracy even at points away from the shock. We remark that in both problems 1 and 2, the resolution achieved by the present scheme is not markedly different from the second-order results.

PROBLEM 3. In this case we compute $M = 1.4$ flow through a channel that has a 4% parabolic hump on the bottom wall. This problem has been used as a test case for many other algorithms. The main features of the flow are the reflection of the leading edge oblique shock from the upper wall and its interaction with the oblique shock emanating from the trailing edge. Figure 3 shows the computed Mach contours on a 120×60 grid, using the second-order TVDSYM. The reflected shock from the top wall interacts with the oblique shock from the trailing edge, giving rise to two triangular regions of uniform flow separated by a shock which hits the bottom wall. This reflected shock from

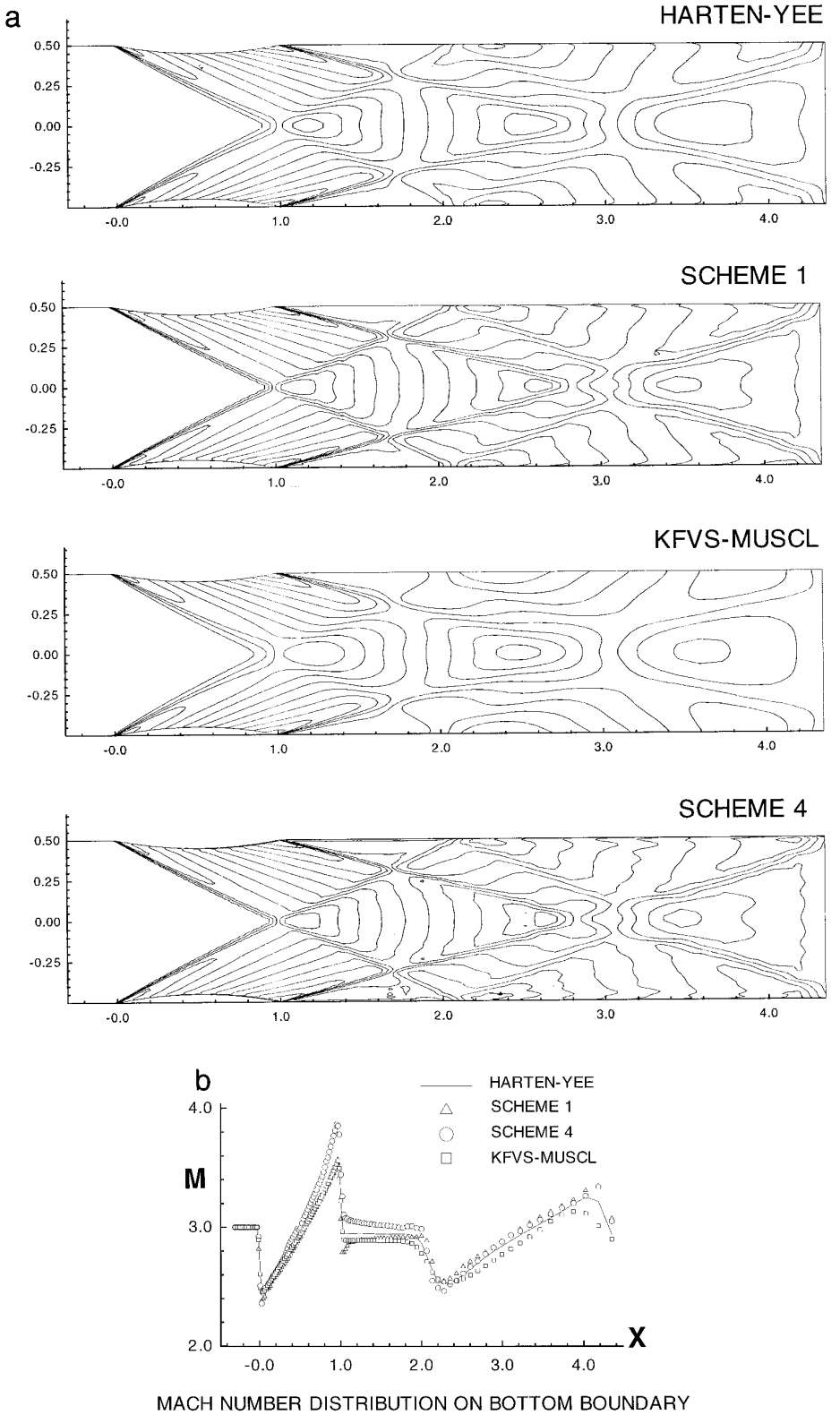

FIG. 4. Flow in convergent–divergent channel. Isomachs NC = 20, DM = 0.09.

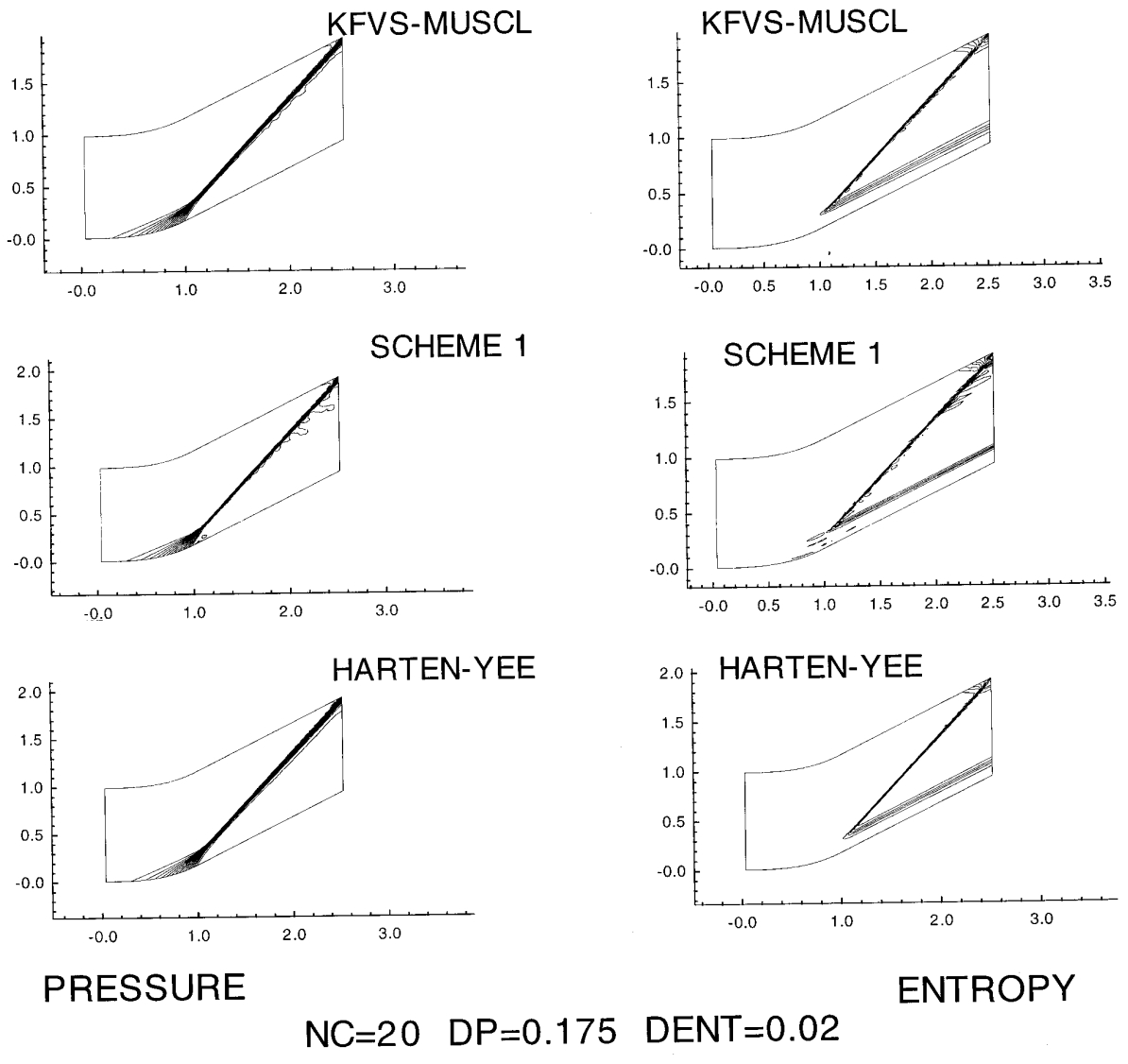

FIG. 5. $M = 3.0$. Flow past a curved wall.

the bottom wall subsequently merges with the trailing edge shock which reflects back and forth until it becomes considerably weakened at the exit. The bottom surface Mach number distribution shows the captured shocks clearly. These are sharp and free of wiggles. Note that the shock transitions computed by CUD-TOL are sharper, especially downstream of the hump, showing the higher resolution achievable by the present schemes. Also the Mach number distribution ahead of the trailing edge shock has slightly higher peaks for the present schemes, perhaps due to the smaller dissipation, as compared to the second-order TVDSYM.

PROBLEM 4. Figure 4a shows the isomach contours for $M = 3$ flow through a converging–diverging channel using the following schemes: (i) second-order upwind Harten–Yee (flux-difference splitting); (ii) second-order KFVS–MUSCL postprocessing; (iii) CUD-TOL (third order); and (iv) CUD-MAFU (fifth order). Note that while the MUSCL postprocessing approach gives inferior shock resolution compared to that of the Harten–Yee upwind scheme, the compact scheme shock transitions are much better resolved, especially in the interaction regions downstream of the channel. The surface Mach number and Cp distributions shown in Fig. 4b also confirm these observations.

Figure 6 shows a comparison of the pressure contours obtained using the KFVS-MUSCL scheme and the present scheme on 120×60 and 90×40 grids, respectively. The

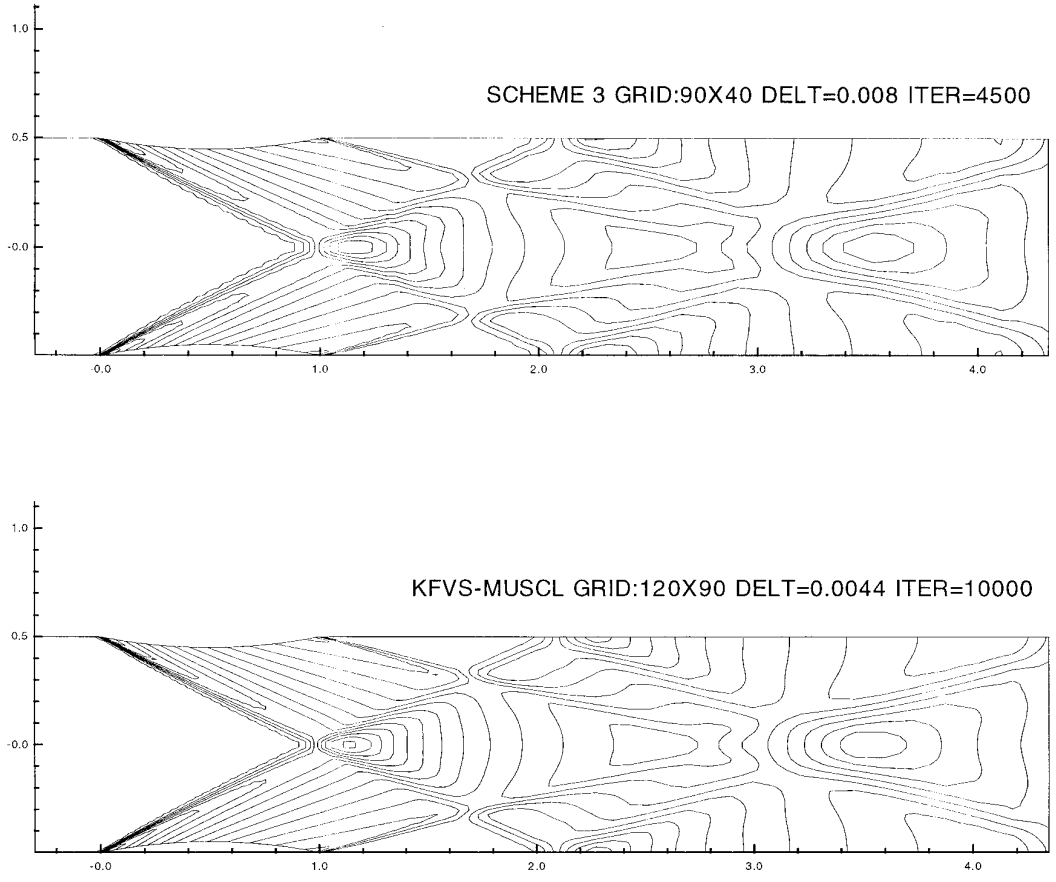

FIG. 6. $M = 3$. Flow in C-D channel, pressure contours. Comparison of Scheme 3 with KFVS-MUSCL, NC = 20, DP = 0.1.

KFVS-MUSCL scheme took about 10,000 time steps for the residual to drop by three orders of magnitude while with the present scheme 1 a residual drop of four decades was achieved in about 4500 time steps. Numerical experiments reveal that on a given grid, the CPU seconds required by the present scheme per time step is about three times that needed by the KFVS-MUSCL scheme. This directly corresponds to the 3-stage Runge–Kutta scheme used for time marching in the compact algorithms. This also implies that the present postprocessing approach for generating the higher order fluxes, Eq. (2.11c), is only slightly more expensive than the conventional MUSCL approach. This indicates that the compact algorithms may be made more attractive computationally if one can fully exploit the scope of the multistage schemes by increasing the stability range using techniques such as implicit residual smoothing.

PROBLEM 5. Last, in Fig. 5 we present the results for $M = 3$ supersonic flow past a curved channel. Zeroth-order extrapolation is used on the upper computational boundary for this calculation. The problem is a simple test case for generating a contact discontinuity in the interior of a flow field. The objective in computing this problem was to see if the present compact schemes can resolve the contact discontinuity any better than the second-order upwind schemes. It is apparent from Fig. 5, however, that the present scheme in this respect performs only marginally better than the second-order schemes:

6. CONCLUSIONS

High order compact upwind schemes for the compressible Euler equations in general geometries have been formulated. Upwinding is incorporated through flux-vector splitting. With the introduction of minmod flux limiters, these schemes are shown to be TVD for the case of a scalar conservation law in one space dimension. These spatial discretizations have been combined with three-stage TVD Runge–Kutta time marching to obtain an explicit family of schemes that may be used for steady state computations. In the present work we have used the KFVS split fluxes in actual numerical computations. Computed results show that higher accuracy and resolution is indeed achievable via the postprocessing approach using compact upwind difference operators and split fluxes.

ACKNOWLEDGMENTS

This work was done as part of the Indo-Russian ILTP programme and was supported by the Department of Science & Technology, Goverment of India. The computing facilities extended by the Experimental Aerodynamics Division and the corporation of the staff at the VAX computing center is gratefully acknowledged. The author thanks anonymous reviewers for comments that improved the quality of this paper.

REFERENCES

1. S. Lele, *J. Comput. Phys.* **103,** 16 (1992).
2. J. C. Mandal and S. M. Deshpande, *Comput. & Fluids* **23,** 447 (1994).
3. A. I. Tolstykh, *Dokl. Akad. Nauk SSSR* **210,** 48 (1973).
4. A. I. Tolstykh, *Current Problems in Computational Fluid Dynamics,* edited by O. M. Belotserkovskii and V. P. Shidlovsky (MIR, Moscow, 1975).
5. A. I. Tolstykh and K. S. Ravichandran, NAL TM CF 9101, 1991 (unpublished).
6. K. S. Ravichandran, NAL PD CF 9401, 1994 (unpublished).
7. K. S. Ravichandran, *Int. J. Comput. Fluid Dyn.,* submitted.
8. S. Abarbanel and A. Kumar, NASA CR 181625, ICASE Rep. No. 88-13, 1988 (unpublished).
9. M. H. Carpenter, *12th ICNMFD*, Lect. Notes in Phys., Vol. 371, p. 254, edited by K.W. Morton (Springer-Verlag, New York/Berlin, 1990).
10. B. Cockburn and C. W. Shu, NASA CR 189663, ICASE Rep. No. 92-21, 1992 (unpublished).
11. Ma Yanwen and Fu Dexun, *Proceedings 5th ISCFD, Sendai, Japan, 1993.*
12. H. Yee, NASA TM 101088, 1989 (unpublished).
13. A. I. Tolstykh and D. A. Shirobokov, *Proceedings, First Asian, CFD Conf., Hong Kong, 1995.*
14. K. S. Ravichandran, NAL-PD-CF 9413, 1994 (unpublished).
15. E. Tadmor, *SIAM J. Numer. Anal.* **25,** 5 (1988).
16. D. W. Halt and R. K. Agarwal, *AIAA J.* **30,** 8 (1992).
17. J. Y. Yang *et al*., *12th ICNMFD*, Lect. Notes Phys., Vol. 371, p. 248, (Springer-Verlag, New York/Berlin, 1990).
18. S. P. Spekreijse, *Proefschrift* (Centrum voor Wiskunde Informatica, Amsterdam, 1987).